HOSTED BY
ELSEVIER
Available online at www.sciencedirect.com
ScienceDirect
Soils and Foundations 63 (2023) 101252
SOILS AND FOUNDATIONS
www.elsevier.com/locate/sandf

Technical Paper

Geotechnical characterization of collapsible salty sands subjected to monotonic and cyclic loadings – A case study for areas with high seismicity

Jorge Macedo [a], Gavi Sotelo [b], Susana Orellana [c], Luis Vergaray [a], Fangzhou Liu [d] Hamza Jaffal [e], Chadi El Mohtar [c]

[a] School of Civil and Environmental Engineering, Georgia Institute of Technology, Atlanta, GA, USA
[b] Knight Piésold Consulting, Lima, Peru
[c] Department of Civil, Architectural, Environmental Engineering, University of Texas at Austin, Austin, TX, USA
[d] Department of Civil and Environmental Engineering, University of Alberta, Edmonton, AB, Canada
[e] Golder Associates Inc., Atlanta, GA, USA

Received 25 December 2021; received in revised form 27 November 2022; accepted 30 November 2022

Abstract

Collapsible soils are typically found in arid regions and often have an aeolian or alluvial origin. In their natural states, they may have a low moisture content and cemented structure that can contribute to high strength and stiffness; however, wetting or saturation can reduce the strength and stiffness due to loss of the cementation. This paper presents a geotechnical characterization of collapsible salty sands in the highly seismic southern coast of Peru, which makes the characterization of their dynamic properties and expected response to earthquake-induced demands (e.g., liquefaction) of primary importance. The geotechnical characterization was performed on intact and remolded samples utilizing various field and laboratory tests, including oedometer, direct shear, static triaxial, cyclic direct simple shear, torsional resonant column, plate loading, and MASW tests. The results revealed insights on the geotechnical properties and mechanical response of collapsible soils and the effects of salt cementation. The results indicated: 1) a decreasing brittle and collapsible behaviors with decreasing cementation while maintaining consistent post-collapse residual strength; 2) oedometer and in situ plate loading tests showed a sudden increase in deformations once cementation is broken; 3) higher dilation potential of collapsible soils as compared to natural sands; 4) decrease in the maximum shear modulus due to the loss of cementation; 5) increase in the stress dependence of the maximum shear modulus with loss of cementation; and 6) a higher resistance to liquefaction for the collapsible soils, even after washing, as compared to natural sands, which may be ascribed to the more pronounced dilation potential.

Keywords: Collapsible soils; Brittleness; Static and cyclic strength; Salt cementation; Dynamic properties; Dilation potential

1. Introduction

The term collapse in granular materials is used to describe a sudden and significant deformation; it is not the immediate settlement nor primary (or secondary) consolidation settlement (Mackechnie, 1989). The typical features of collapsible soils include open structure, high void ratio, low dry density, high sensitivity, low inter-particle strength, and geologically young or recently altered materials (Rogers, 1995). Collapsible soils are typically found in arid regions and often have an aeolian or alluvial origin; they often have low moisture contents with high initial or peak shear strength due to cementation. However, they can suddenly show a collapse when subjected to a major

Peer review under responsibility of The Japanese Geotechnical Society.

https://doi.org/10.1016/j.sandf.2022.101252

List of Symbols

Symbol	Description
Pa	Atmospheric Pressure
I_b	Brittleness Index
I_e	Collapse Index
$\sigma_3\prime$	Confining effective stress
$N1_{60}$	Corrected blow count number
CSR	Cyclic Stress Ratio
q	Deviatoric Stress
χ	Dilatancy Index
$\phi\prime$	Effective friction angles
n_G	Exponential fitting parameter for Shear modulus function of confining stress
A_g	Fitting parameter for Shear modulus function of confining stress
F3PV	Flushed with 3 pore volumes
F9PV	Flushed with 9 pore volumes
I	Intact
$\sigma\prime$	Isotropic confining effective stress
ψ_0	Initial state parameter
G_{max}	Low amplitude Shear modulus
D_{min}	Maximum Dilatancy
$p\prime$	Mean stress
MASW	Multichannel Analysis of Surface Waves
$\sigma'_1, \sigma'_2, \sigma'_3$	Principal effective stresses
Su_y	Peak shear strength
RC	Reconstituted
RW	Reconstituted Washed
Dr	Relative density
Su_r	Residual shear strength
S1	Sample 1 from collapsible soil type B
S2	Sample 2 from collapsible soil type B
S3	Sample 3 from collapsible soil type B
G	Shear modulus
V_s	Shear wave velocity
B	Skempton pore pressure parameter
SPT	Standard Penetration Test
η	Stress ratio
M_{tc}	Stress ratio at critical state
σ_v	Vertical total stress
e	Void ratio

increase in water saturation. Common cementation agents are salt (Fan et al., 2017), carbonate (Schanz et al., 2018, Milodowski et al., 2015, Al-Saoudi et al., 2013), and clay (Smalley et al., 2006, Rinaldi et al., 1998).

Collapsible soils impose a variety of geotechnical/geological hazards associated with their collapse potentials, such as causing undesired settlements in infrastructure (Noutash et al., 2010; Sakr et al., 2008; Vandanapu et al., 2016) or slope instabilities (Derbyshire and Mellors, 1988; Qi et al., 2018; Xu et al., 2018). Cerato et al. (2009) indicated that the factors affecting the collapsible potential of soils are initial moisture content, initial dry density, soil composition, and confining pressure. Field tests are often used to identify collapsible soils and characterize their collapsible potential (Al-Rawas, 2000; Houston et al., 2001; Kalantari, 2013). Common full-scale field tests include some type of plate loading tests (e.g., down-hole collapse test), which are used to obtain load–displacement responses of the soil at various wetting conditions (Houston et al., 1995; Reznik, 1993). Site characterization techniques, such as standard penetration test, cone penetration test, and seismic and electromagnetic waves, have also been used to assess correlations of index properties with collapsible potential (Hailemariam et al., 2015; Houston et al., 2001; Rinaldi et al., 1998; Rollins et al., 1998).

Previous studies on collapsible soils have been centered on understanding the collapse mechanisms for ground improvement (e.g., Assadi-Langroudi, 2014; El Howayek et al., 2011; Houston et al., 2001). Al-Rawas (2000) emphasized the roles of open fabric, grain-cement connection, and matrix suction on collapse mechanisms. Li et al. (2016) categorized three typical approaches to analyzing the collapse mechanism, including traditional collapse indexes, microstructure analyses, and unsaturated-based approaches. Traditional indexes describe collapse by one or several soil properties (Feda, 1988, 1966). Microstructure-based efforts rely on image techniques to characterize fabric change (Delage et al., 1996; Li et al., 2018; Liu et al., 2015). Unsaturated-based assessments attribute the collapse to suction reduction and use constitutive models to predict collapse behavior (Alonso et al., 1990; Cui and Delage, 1996; Fredlund and Gan, 1995).

Various studies have also evaluated the overall volume-stress change of collapsible soils in the context of geotechnical characterization, including both natural collapsible soils (Cui et al., 2004; Karam et al., 2009; Song et al., 2017) and compacted soils (Haeri et al., 2014; Rampino et al., 2000; Sivakumar and Wheeler, 2000; Wang et al., 2002; Zhou and Sheng, 2009). For a natural collapsible soil, comparing the mechanical behaviors of its intact and reconstituted states can provide insights into the effects of structure (e.g., Xu and Coop, 2016), as the reconstituted specimen contains facets of the behavior of the main constituents of the soil. The mechanical behaviors of collapsible sands are of interest to engineering applications, and in particular, for the construction of critical infrastructures, e.g., tailing dams (Sotelo and Paihua, 2017). However, limited studies are available on analyzing the volume-stress change of natural collapsible sands, and to the best knowl-

edge of the authors, there are no previous studies evaluating the coupling between their static and cyclic responses.

This study presents the geotechnical characterization of a natural collapsible salty sand in a seismic region of southern Peru, where a Tailing Storage Facility (TSF) will be constructed, expanding on preliminary results and discussions presented in Sotelo et al. (2019). The collapsible sand has a metastable structure with large voids and a skeleton of grains that are cemented by salt precipitate residues and are expected to be affected by monotonic and earthquake loadings. An extensive laboratory and field characterization program was conducted to characterize the static and cyclic response of these collapsible sands and provide useful insights into the relatively uncharacterized behavior of these collapsible materials.

2. Study area and overview of geotechnical characterization

The study area is located in an arid and highly seismic region on the southern coast of Peru, part of the Pacific Ring of Fire. The regional tectonic framework on a larger scale is governed by the interaction of the Nazca and South American plates. The border between the Nazca Plate and the South American Plate in this region is demarcated by the Peru-Chile trench. The continuous subduction of the Nazca plate along the Peru-Chile trench is the main source of large earthquakes ($M > 7.0$). The lithology consists of alluvial and aeolian deposits up to 13 m in thickness, including the collapsible soil formed by the accumulation of sediments in a dry and evaporative environment. Collapse-induced deformation is a concern due to the considerable thickness of the present collapsible soils and the seismicity of the site, and thus an understanding of the collapse mechanisms and geotechnical properties are of primary importance.

The geotechnical site investigation for the study area consisted of 39 boreholes and 152 test pits executed between 2007 and 2017, including in-situ field testing and sampling. Fig. 1 shows a panoramic view of the study area. During the site investigation, intact and disturbed samples were extracted for material characterization in the laboratory. The intact samples were obtained in the form of block samples, with approximately 300 mm × 300 mm × 150 mm. Fig. 2 shows an example of the recovered intact block samples. These samples were used to perform laboratory tests, including oedometer, direct shear, consolidated undrained and consolidated drained (CU/CD) triaxial, resonant column, and cyclic direct simple shear (CDSS) tests. The disturbed samples were collected from boreholes and test pits for index testing, including Atterberg limits, particle size distribution, specific gravity, and soluble salts content tests. In-situ field testing included Standard Penetration Tests (SPT), shear wave velocity measurements using Multichannel Analyses of Surface Waves (MASW), downhole permeability tests (Lefranc tests), and plate loading tests.

3. Collapsible soil characterization

3.1. Index properties

Index properties, such as gradation, moisture content, salts content, and collapse index, were obtained for the collapsible soil. The soil is mainly classified as poorly graded sands (SP) and silty sands (SP-SM) with low natural moisture content. Fig. 3 shows the range of particle size distribution curves for the recovered samples. The collapsible sand was sub-divided into two types, collapsible soils Type A and B. Fig. 4 shows the variation between the void ratio and depth for the two types of collapsible soils. The void ratio was estimated in the laboratory from recovered samples and also from field tests. Sand cone tests, densimeter tests, and specific gravity tests were performed to estimate the in-situ void ratio. Collapsible soil Type A generally extends from 3 m to 8 m depth (with variable depths depending on the location within the valley); it has a void ratio greater than 0.7 in most cases and is underlain by Collapsible soil Type B, which has a void ratio mostly lower than 0.7. The distinction between the two layers was also confirmed with shear wave velocity vertical profiles, as shown later in Fig. 6b.

Fig. 1. Panoramic view of the study area.

Fig. 2. Intact block samples. The arrows correspond to the vertical direction in-situ.

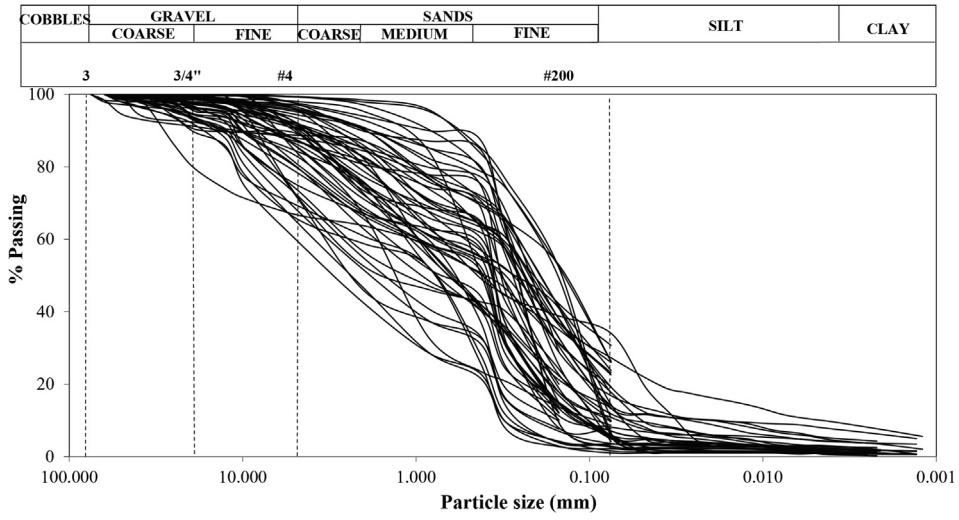

Fig. 3. Particle size distribution of the collapsible soils considered in this study.

3.2. Collapsibility and salt content

The standard test method for measuring the collapse potential of soils (ASTM D5333-03) was conducted to obtain the collapse index (I_e), which is defined as the difference between the strains before and after wetting at a vertical stress of 200 kPa, under a conventional 1-D oedometer loading condition. Fig. 5**a** shows the results of all the oedometer tests performed to measure I_e, where it can be observed that collapsible soil Type B specimens experience minimal decrease in void ratio, compared to collapsible soil Type A specimens, after the wetting at the 200 kPa vertical stress. Fig. 5**b** summarizes the variation of the calculated I_e for collapsible soils Type A and B, relative to their initial void ratio. The I_e values vary from 0.7 % to 14 % for type A (i.e., slight to severe collapsibility degree), whereas the I_e values for type B are in the range of 0.4 % to 0.5 % (i.e., slight collapsibility degree).

Precipitated salts were identified as the cementing agent bonding the soil particles to produce their brittle structure. The standard test NTP 339.152 (INDECOPI, 2002) was conducted to quantify the salt content relative to the dry mass of sand per each intact block sample. Fig. 5**c** shows the variation of I_e versus salt content for collapsible soils Type A and B. For collapsible soil type A, when the salt content is less than 10 ppm, the collapsibility degree is slight to moderate with few outliers; whereas when the salt content is greater than 10 ppm, the collapsibility degree tends to be moderate to severe. For collapsible soil type B, the collapsibility degree is slight for a salt content within a range of 5 to 15 ppm. Fig. 5**d** shows the relationship between the void ratio and salt content, grouped by

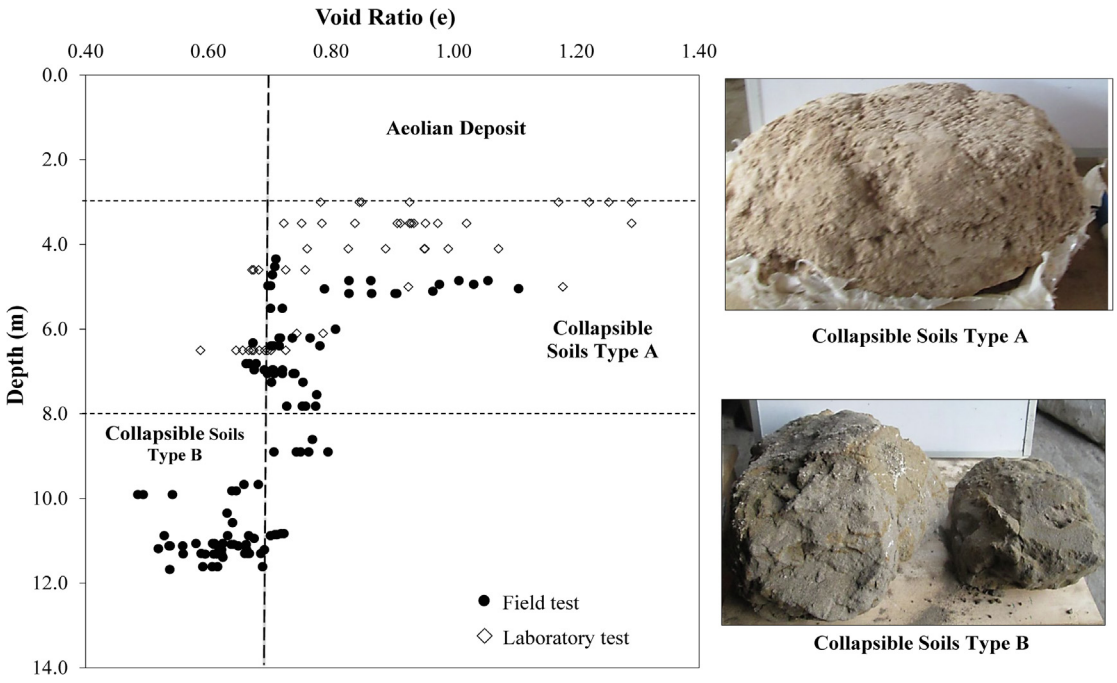

Fig. 4. Void ratio vs depth for collapsible soils Type A and B.

schematic I_e contours. Of note, only the tests at 200 kPa where I_e is defined are considered. Based on the available data, it can be seen that there are apparent I_e contours for collapsible soil type A where I_e increases as the void ratio and the salt contents, which is consistent with the previous discussions. In the case of collapsible soil type B, the variation of salt content is less pronounced; hence, all I_e values are grouped in the "slight" category.

Field tests included the standard penetration test (SPT), multichannel analysis of surface waves (MASW) test, Lefranc permeability test, and plate loading test. Cone penetration tests (CPT) were not possible due to refusal at the surface. SPTs were performed in dry conditions (in-situ condition) and also after wetting. The wet conditions were created by flooding the borehole during saturation for the permeability tests (prior to SPT tests) with 2–3 additional hours of saturation. In the dry condition, the number of blow counts was higher than 50 in most cases with few instances reporting blow counts between 30 and 50; hence, indicating a moderately dense to dense compactness. In contrast, in the wet conditions, the blow counts were more sparse varying from 3 to refusal, suggesting a loose to dense compactness. Of note, a complete wetting was not achieved in most SPTs, resulting in high blow counts values, which likely represent a "pre-collapse" stiff condition. Fig. 6**a** presents corrected blow count numbers ($N1_{60}$) under wet conditions (blow counts for the dry condition are not presented as they correspond to refusal in most cases) and a dilative-contractive boundary versus depth in wet conditions (after flooding the borehole). The dilative-contractive boundary for wetted soils during shearing was assessed following the procedures proposed by Fear and Robertson (1995), who proposed boundaries to separate contractive and dilative behavior based on blow count numbers. This boundary shows that the wetted soil is primarily dilatant, and in a few cases, contractive, which again suggests that there may be insufficient wetting as previously discussed and, therefore, the measured values may be still reflecting the cemented dilative response. Fig. 6**b** summarizes the results of shear wave velocity (V_s) measurements. The results show three units; the first unit corresponds to Aeolian deposits from 0 to 3 m with V_s between 250 and 300 m/s. This unit is followed by collapsible soils Type A from 4 to 8 m with V_s between 300 and 350 m/s. Finally, there is an additional unit that corresponds to collapsible soils Type B with V_s between 400 and 450 m/s. The interpretation of location in depth of the collapsible soils Type A and B falls within the ranges of depths described in Fig. 4. The average shear wave velocity in collapsible soils Type B is consistent with the resonant column results for a similar confinement stress as subsequently discussed in section 4 (Fig. 13a). The permeability test results showed that the hydraulic conductivity of the soil ranges from 10^{-3} cm/s to 10^{-2} cm/s (Fig. 6**c**), indicating a high permeability, which is consistent with the high void ratios measured in the laboratory for specimens carved from the block samples.

In the case of collapsible soils Type A, plate loading tests were performed by initially excavating the aeolian materials on the surface plus 1 m of the disturbed materials, followed by an additional test pit excavation of 0.5 m in depth with a width equal to the diameter of the plate. Similarly, the collapsible soil Type A was removed to carry out the test for the collapsible soil Type B, following the same procedure

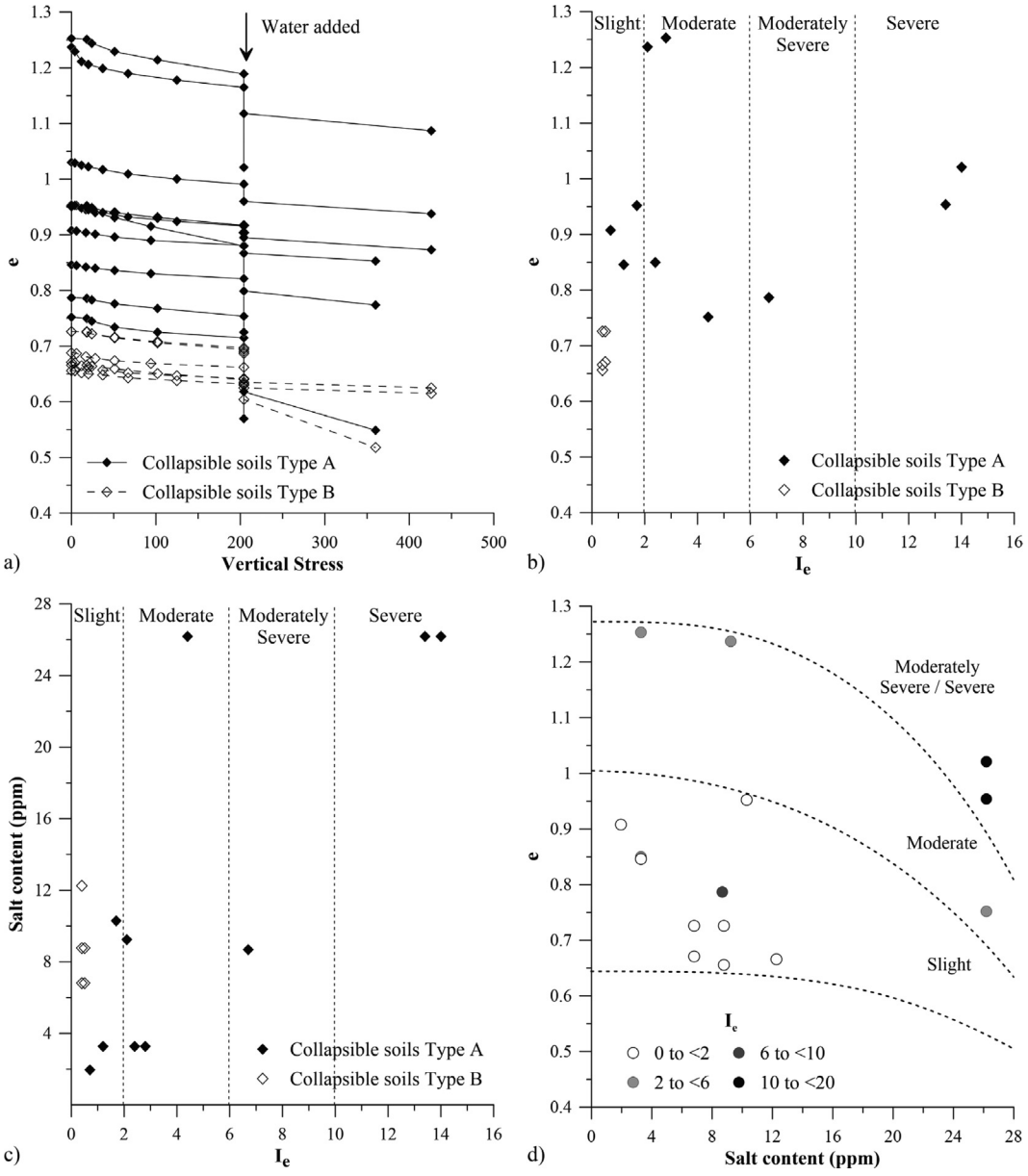

Fig. 5. Collapsibility testing a) Oedometer test results with wetting at 200 kPa, b) collapse index vs void ratio, c) collapse index vs salt content, and d) salt content vs void ratio with collapse index contours.

described above (i.e., an excavation until the desired depth is reached). The bearing plate used was 463 mm in diameter and 25 mm thick. A 20-ton loaded truck, lifted by one set of hydraulic jacks to limit possible movement during load application, provided the reaction force for pushing down on the plate during the tests. Three dial gauges were placed in contact with the bearing plate to measure the settlement of the plate, and thus the settlement of the ground. The seating pressure due to the weight of the plate was 4.6 kPa, and then the load application started with increasing the vertical stress to 59 kPa and continued increasing it by approximately 60 kPa increment until the final stress of 840 kPa was reached. As a key component of the procedure, the soil was inundated to evaluate its response upon a possible collapse. In addition, during the site investigation, sand cone, densimeter, and specific gravity tests were performed close to the plate test, which helped to identify the collapsible soils as Type A or B. Fig. 7 shows the load-settlement responses from two sites, which reveals a stiffer response of collapsible soils Type B as compared to Type A. In addition, a sudden increase in settlements can be observed after inundation ($\sigma_v = 416kPa$), which is consistent with the collapsible nature of these materials. The increase in settlements is greater in collapsible soils Type A, which is consistent with its greater collapse potential, as observed in the laboratory tests.

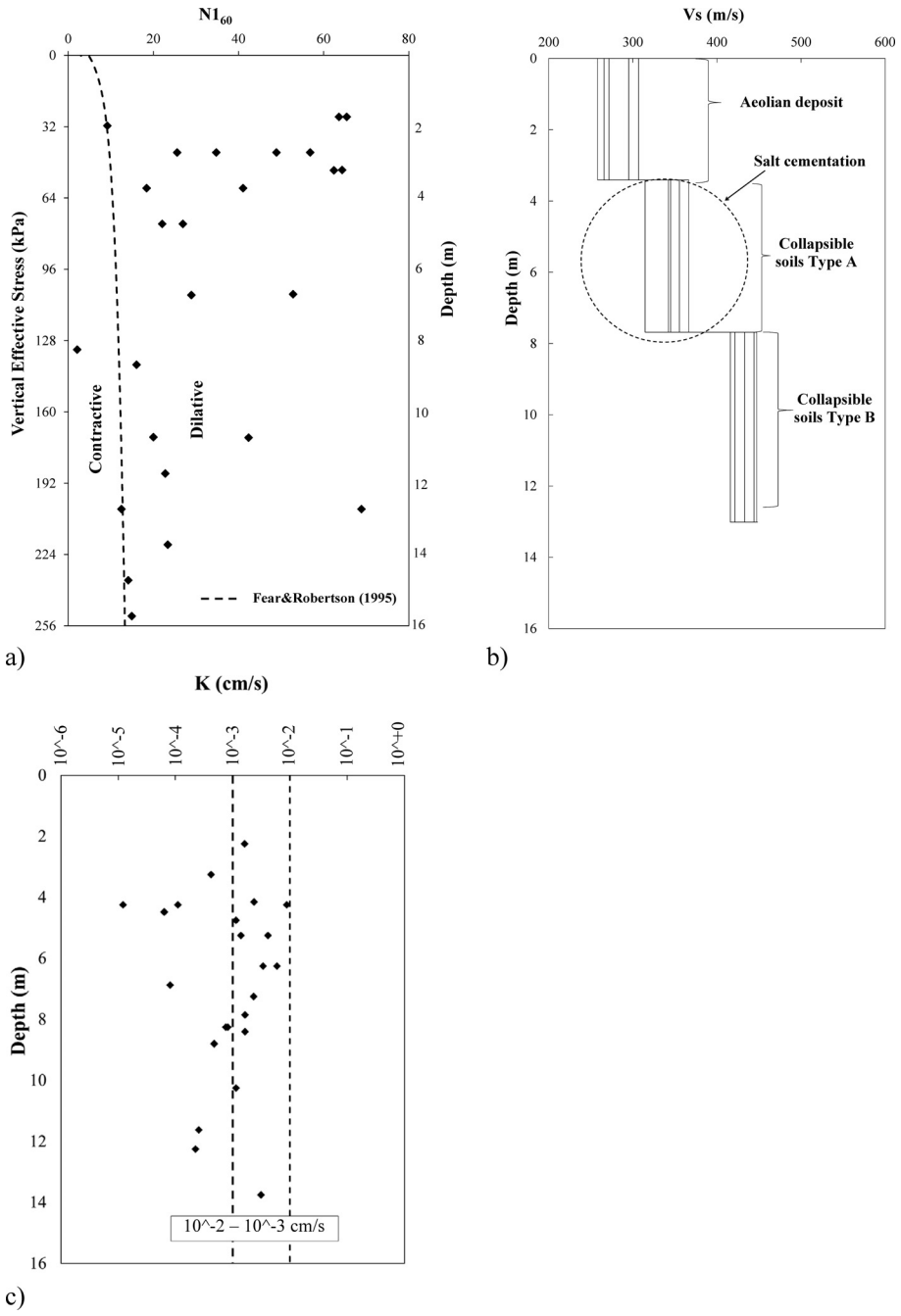

Fig. 6. Results from field tests. a) N160 vs vertical effective stress, b) shear wave velocity vs depth, and c) hydraulic conductivity vs depth.

4. Laboratory test results and interpretation

4.1. Monotonic loading behavior

4.1.1. Direct shear test

The direct shear tests (DS) were performed on intact specimens of collapsible soils Type A and B. The initial dimensions were 5.0 cm in diameter and 2.5 cm in height. The initial conditions (i.e., effective vertical stress, void ratio, and dry density) for each specimen are presented in Table 1. The testing procedures were modified from the standard method to account for the unique nature of this material, as collapse was induced through the wetting of the samples after applying the vertical stress. The vertical deformation was monitored, and the shearing was initiated after the cessation of vertical deformation (i.e., at the end of the collapse). Thus, the shear behavior and strength are representative of a "post-collapse" condition. Fig. 8**a** shows the failure envelopes from these tests, with effective friction angles of $\phi' = 31^{\circ}$ and 36° for soils A and B,

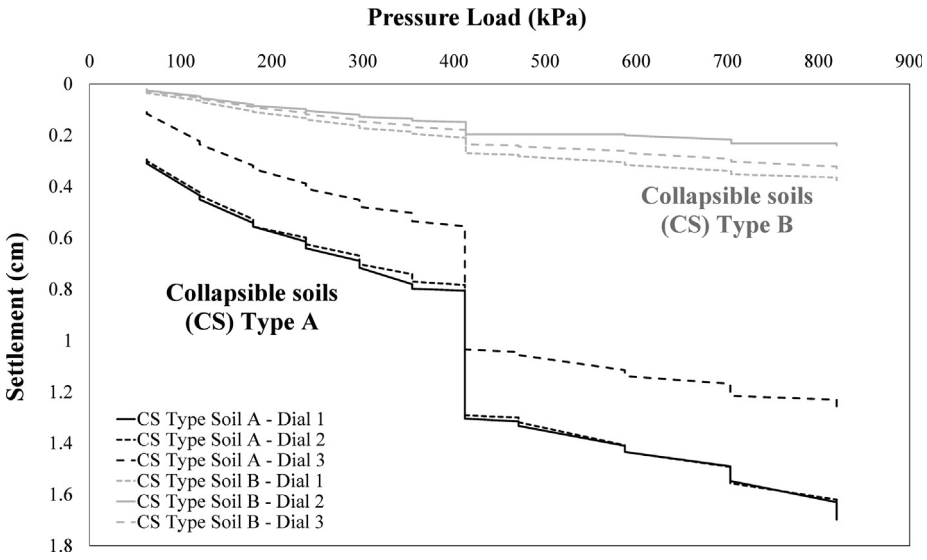

Fig. 7. Pressure vs settlement from plate loading tests.

Table 1
Initial conditions at the beginning of testing for Direct Shear tests.

Specimen ID		Vertical stress (kPa)	Dry density (g/cm^3)	Void ratio
I	Collapsible soils Type A	200	1.20	1.25
		400	1.15	1.35
		600	1.16	1.32
		800	1.18	1.28
	Collapsible soils Type B	200	1.56	0.73
		400	1.56	0.73
		800	1.53	0.76

respectively. Fig. 8**b** presents the horizontal versus vertical displacements during shearing, whereas Fig. 8**c** shows the shear stress evolves in terms of the imposed horizontal displacements. Collapsible soil Type A exhibited contractive behavior over the considered range of stresses. Collapsible soil Type B exhibited dilative behavior at normal stresses of 200 kPa and 400 kPa; however, it exhibited contractive behavior at 800 kPa. This is consistent with the looser nature of collapsible soil Type A, generally showing a contractive behavior. In contrast, collapsible soil Type B is primarily dilative, but it can become contractive at higher normal stresses.

4.1.2. Triaxial test

Given the loose state of collapsible soil Type A, it was not feasible to recover an intact block sample with the required size for a triaxial specimen. Thus, the consolidated undrained (CU) and drained (CD) triaxial tests were performed only on the intact specimens of collapsible soil Type B. These tests were performed to evaluate the mechanical behavior of the collapsible soils with emphasis on the contractive/dilative response of the material upon shearing as the soil transitions from a "pre-collapse" intact state (i.e., cemented) to a "post-collapse" state either by wetting or remolding.

Fig. 9**a, 9b, and 9c** present the deviatoric stress versus axial strain, the development of excess pore water pressures, and the stress paths, respectively. Table 2 presents the initial conditions (void ratios and confinement) for the triaxial tests. The dimensions for the specimens were 6.7 cm in diameter and 14.0 cm in height. The tested specimens were flushed with water and back pressure saturated, achieving B-values in the range of 0.98–1.00. The results in Fig. 9**b** show a tendency to generate negative excess pore pressures (i.e., dilative response) during shearing. The excess pore water pressure levels depend on the confinement stress, which is consistent with the critical state soil mechanics framework**.** CD triaxial tests were also performed in different conditions to evaluate how the collapse affects the strength and stiffness of the tested materials. Table 3 presents the initial conditions for the tests. A detailed description of the aforementioned conditions is given in the following lines:

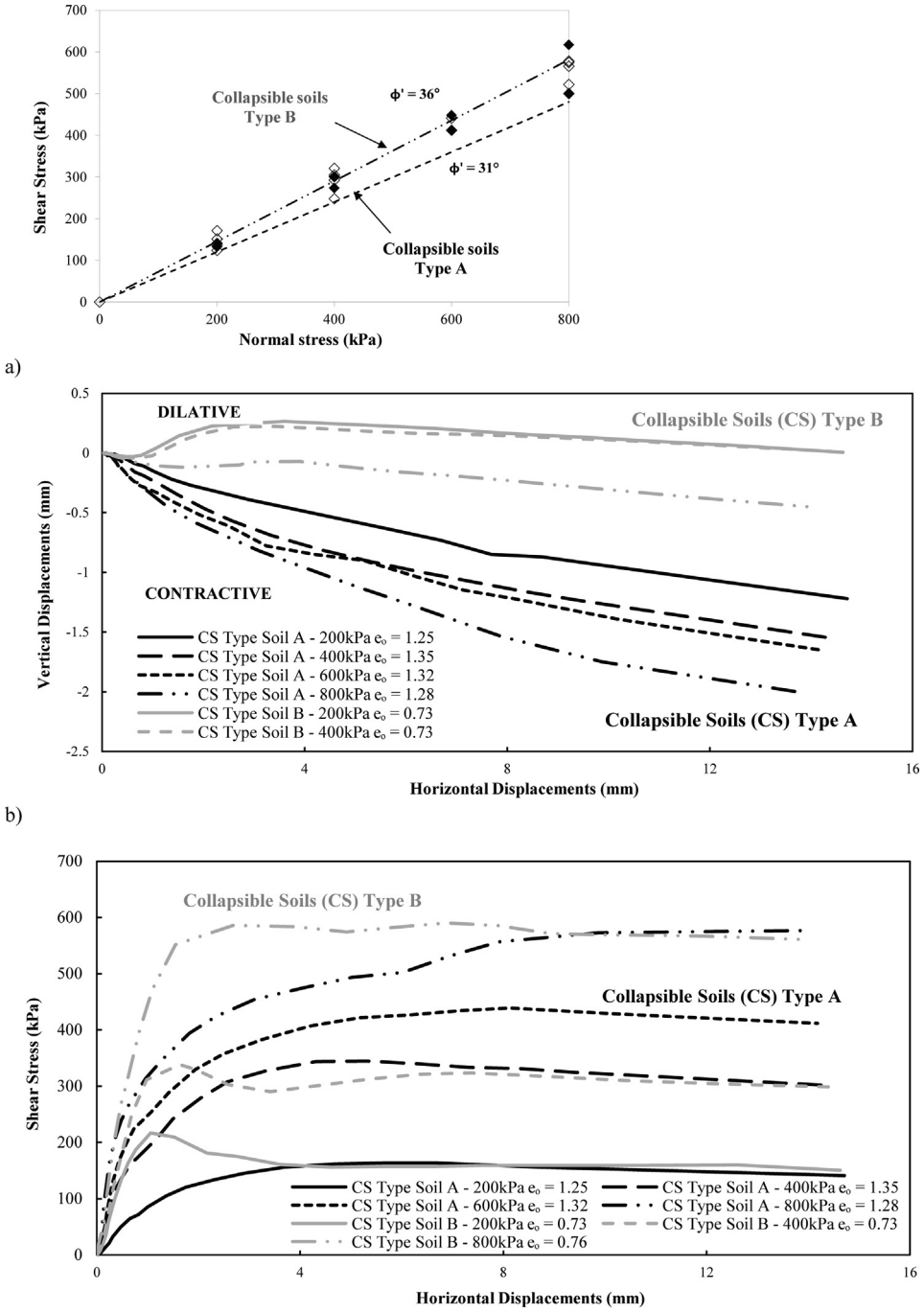

Fig. 8. Direct shear test results for collapsible soils type A and B. a) Failure envelopes in the normal vs shear stress space; b) vertical vs horizontal displacements; and c) shear stress vs horizontal displacements.

a) On intact specimens (I): Specimens at natural water content without any flushing.
b) On intact flushed specimens (F): The specimens were flushed prior to backpressure saturation with 3 and 9 pore volumes (F3PV and F9PV). For the F9PV, 3 pore volumes were flushed at three stages spaced at 2 h. The intent was to remove salt content and increase collapse during consolidation.
c) On reconstituted crushed (RC) specimens and the reconstituted washed (RW) specimens: The RC specimen refers to the condition where the intact specimens were crushed using a rubber mullet with the salt kept in the sand and finally reconstituted. The RW condition refers to the condition where the materials were crushed and then washed to remove the salt (without losing any of the fines)

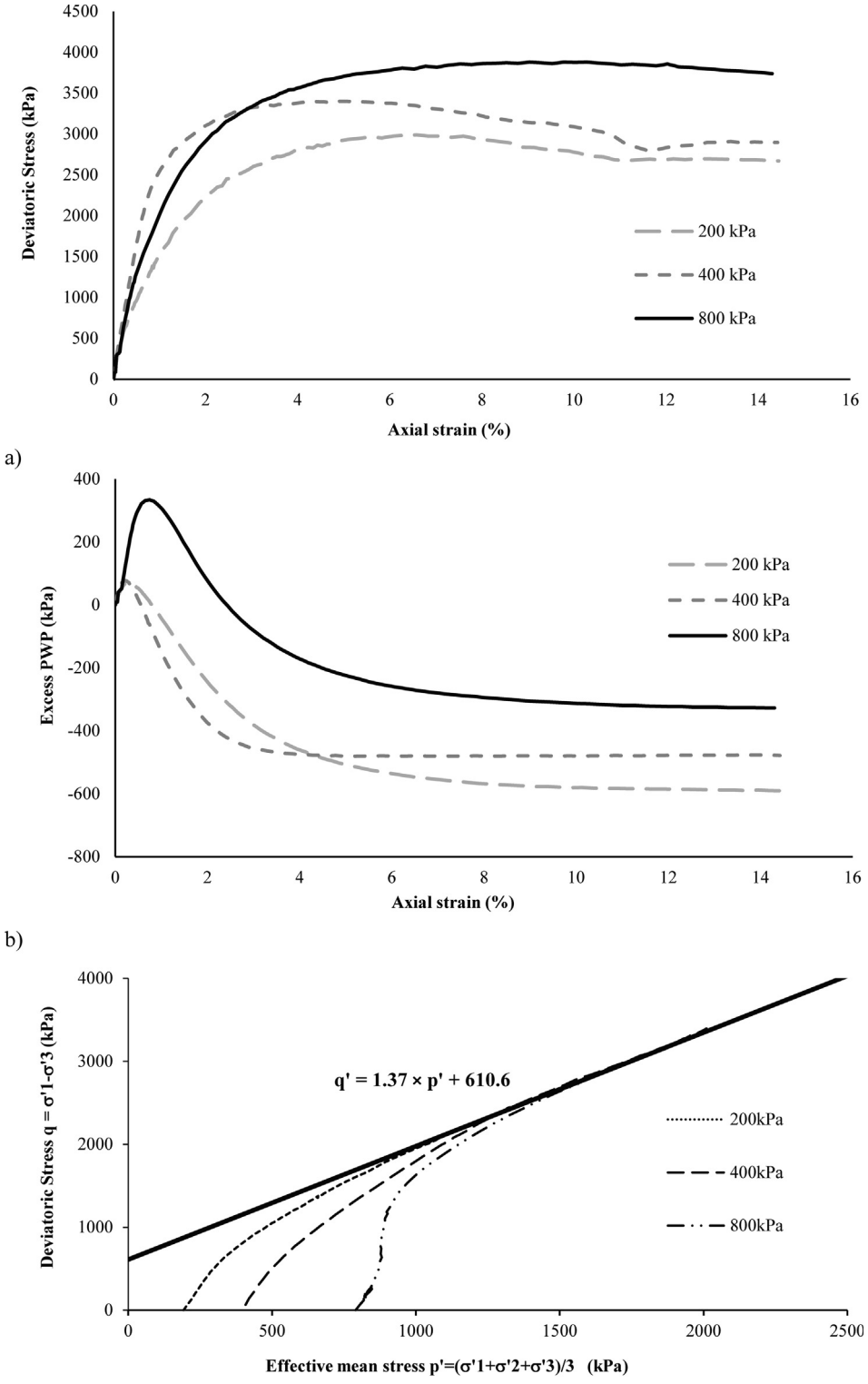

Fig. 9. CU triaxial test results for intact collapsible soils Type B. a) Deviatoric stress vs axial strain; b) excess pore water pressure vs axial strain; and c) stress paths in the p-q space.

and finally dried. In both cases, the specimens were reconstituted at the original dry density of the intact specimens.

The CD tests under I, F3PV, and F9PV were performed on intact block samples, labeled as "S1", "S2", and "S3", based on their location on the extracted intact block

Table 2
Initial conditions at the beginning of testing for TX CU tests.

Specimen ID		Confining stress (kPa)	Dry density (g/cm^3)	Void ratio
I	Collapsible soils Type B	200	1.65	0.64
		400	1.63	0.65
		800	1.63	0.66

Table 3
Initial conditions for TX CD tests on Collapsible Soil Type B.

Specimen ID		Confining stress (kPa)	Dry density (g/cm^3)	Void ratio
I	S1	200	1.62	0.64
		400	1.59	0.67
	S2	400	1.62	0.64
F-3 V	S1	200	1.60	0.65
		400	1.60	0.66
	S2	800	1.63	0.63
F-9 V	S2	200	1.63	0.63
		400	1.63	0.63
		800	1.63	0.63
	S3	200	1.62	0.64
		400	1.62	0.64
		800	1.61	0.65
RW	S1/3	200	1.62	0.64
		400	1.58	0.67
		800	1.61	0.64
RC	S1/3	200	1.59	0.69
		400	1.57	0.69
		800	1.63	0.63

samples. In addition, CD tests under RC and RW conditions were performed by combining S1 and S3 samples (the combination was labeled as S1/S3) as both samples showed similar responses under intact conditions (I).

Fig. 10**a** compares the stress–strain responses of S1 and S3 at 200 kPa for I, F9PV, F3PV, and RW conditions. The results show a decrease in brittleness as the cementation is removed. Bishop (1971) defined the brittleness index as $I_b = (Su_y - Su_r)/Su_y$, where Su_y is the peak strength and Su_r is the residual strength. The brittleness indices of the I, F3PV, F9PV, and RW specimens were 0.70, 0.47, 0.24, and 0.13, respectively. This suggests the more water flushing occurs; the more salt is washed out of the specimen, which in turn, reduces the remaining cementation as well as the peak strength and brittleness. Interestingly, I_b shows a significant change when transitioning from the I specimen to the F3PV specimen, but not an important change after the flushed F9PV specimen, suggesting that there was not a significant decrease in cementation after the F9PV flushing. Fig. 10**b** shows similar results for the specimens tested at 400 kPa, which also reveal similar observations. Fig. 10**c** shows results for the S2 sample tested at 400 kPa for I and F9PV specimens, the stress–strain of a I-S1 specimen (i.e., I specimen from sample S1) tested at the same confinement is also shown for comparison. The I_b value for the I-S2 specimen is 0.43 (lower than $I_b = 0.60$ for the I-S1 specimen at the same confinement), suggesting lower cementation compared to specimens S1 and S3. The I_b value for the I-S2 specimen is higher than the I_b for F9PV-S2 specimen ($I_b = 0.10$), which is consistent with the previous observation on the reduction of cementation due to flushing on specimens S1 and S3.

Fig. 10**d** compares the response of specimens F3PV-S2, and F9PV-S2 at 800 kPa, which shows a similar behavior with I_b values of 0.22 and 0.23, respectively. This suggests that there is no significant further decrease in cementation after the F3PV flushing of the S2 sample. Fig. 10**d** also compares the stress–strain responses for F9PV specimens from S2 and S3 samples at different confinements. The curves illustrate a more brittle behavior in the F9PV-S3 specimens as compared to the F9PV-S2 specimens, which is consistent with the previous results, suggesting higher cementation in the S1 and S3 samples as compared to the S2 sample. Fig. 10**e** compares the stress–strain curves for the reconstituted specimens from samples S1 and S3 (i.e., S1/S3); the RW and RC specimens show a similar response for different confinements, suggesting that crushing and crushing/washing processes may have removed the cementation to a similar degree. In addition, for the crushed and washed specimens, the loss of cementation was found not only to reduce the peak strength and brittleness, which were comparable with F9PV specimens but also to change the evolution of the stiffness in a different pattern as compared to the intact specimens. Fig. 10**f** compares the stress–strain curves of an F9PV-S3 specimen and the RC and RW S1/S3 specimens. The RW and RC specimens exhibited an initial stiff response, which gradually softened until reaching their peak strength. For the intact flushed specimen, the initial stiffer phase remained largely unchanged until the peak stress was reached. The results suggest that the cementation in the RW, RC, and F9PV specimens was removed (similar peak strength for all specimens); however, the microstructure of the RW and RC specimens are different, resulting in a less brittle response as compared to that in the F9PV-S3 specimen.

In terms of the residual strength, the flushing/reconstitution process can be seen as having a minimal impact providing an average friction angle of 38° from all tests (with a variation of +- 1.5°). This is because all the samples were in a "post-collapse" state (at least on the failure plane) by either collapse in the intact specimens, flushing (3PV-9PV flushed specimens), or crushing and washing (crushed and washed specimens). Such an observation suggests that, despite the processes applied, the specimens arrived at a similar residual strength (at the same confinement), which is consistent with the critical state soil mechanics framework (Jefferies and Been, 2015).

To study the contractive/dilative behavior of these materials, their void ratio (e) versus mean stress (p) responses and dilatancy behavior were explored. Fig. 11**a and 11b** show *thee* versus $p\prime$ curves for the S1 and S3 samples, which we plotted together as we observed similar behaviors on their stress–strain curves, whereas Fig. 11**b** shows the e versus $p\prime$ plot for the sample S2. From these

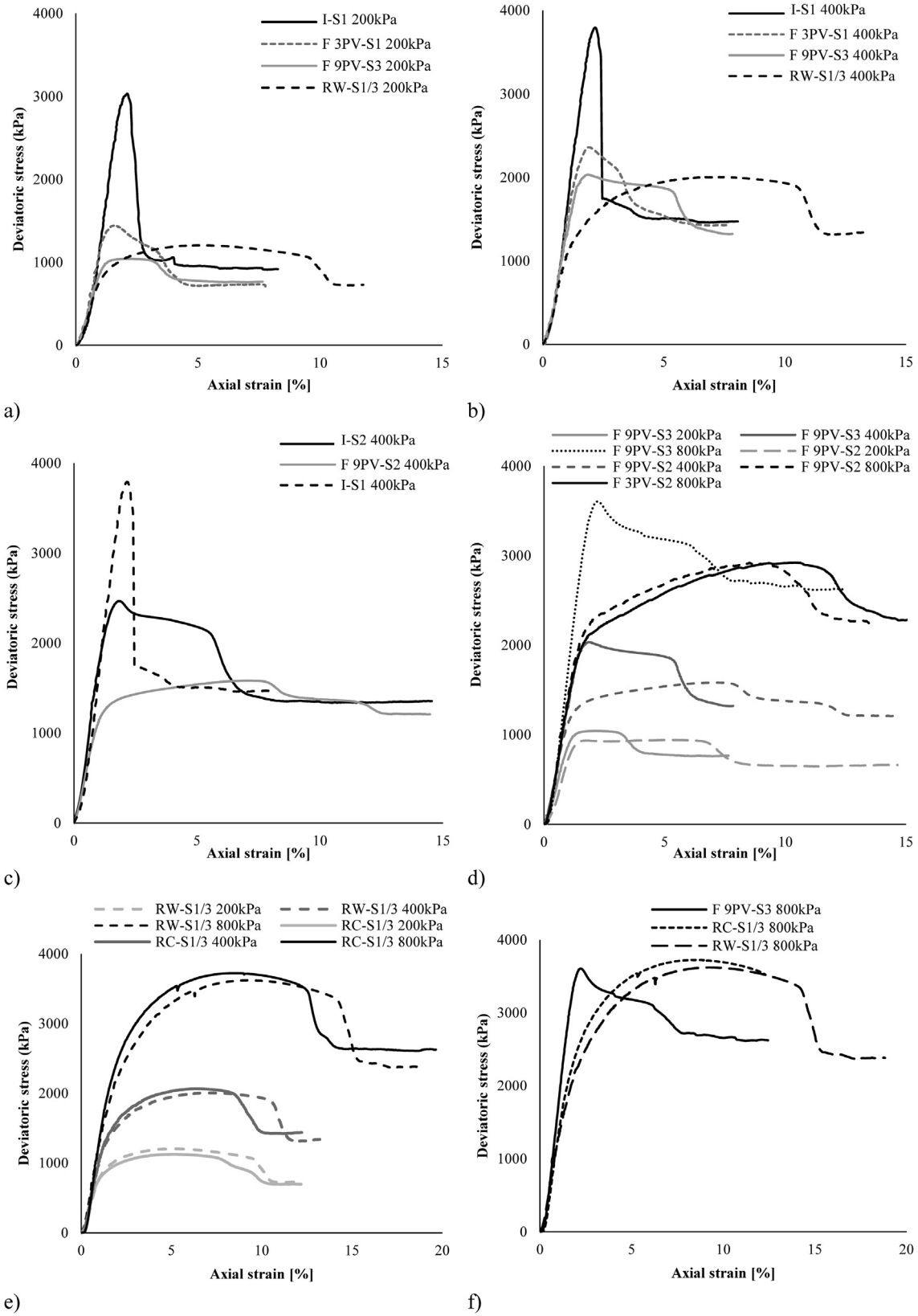

Fig. 10. Stress strain responses for samples S1/S3 and S2 in triaxial CD tests. Response of S1 and S3 samples considering I, F9PV, F3PV, and RW specimens tested at (a) 200 kPa and (b) 400 kPa; c) response of S2 samples, considering I, F9PV samples at 400 kPa; d) response of specimens F3PV-S2 and F9PV-S2 at 800 kPa, and stress–strain response for F9PV specimens from samples S2 and S3; e) stress–strain response of reconstituted (RW, RC) S1/3 specimens; f) stress–strain curves of a F9PV specimen from sample S3 and reconstituted RC, and RW specimens.

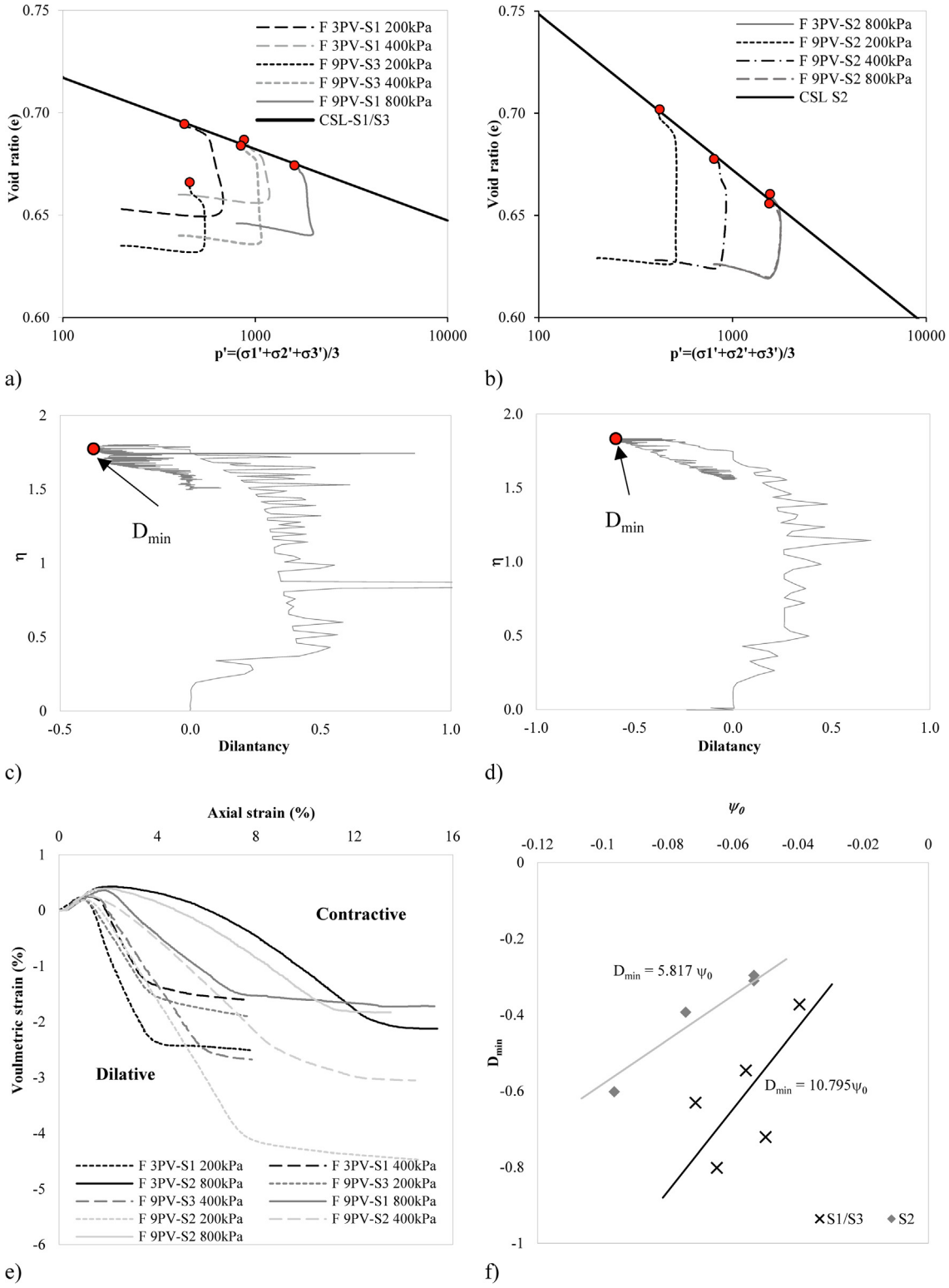

Fig. 11. CSLs in e vs mean pressure space for a) samples S1, S3 and b) sample S2, respectively; c) and d) examples of dilatancy vs stress ratio for samples S1, S3 and sample S2, respectively; e) Axial vs volumetric strain; and f) initial state parameter (ψ0) vs maximum dilatancy (Dmin) for samples S1/S3 and S2.

figures, it can be noticed that the 'end-of-test' points of each test tend to converge over a common line, i.e., towards the critical state lines (CSL). The interpreted CSLs for the S1, S3, and S2 samples are presented in Fig. 11**a and 11b**. The samples S1 and S3 tend to converge to the same CSL as they were recovered from the same location,

whereas the material S2 shows a different CSL. This is consistent with the similar cementation and stress–strain behaviors observed in samples S1 and S3. Fig. 11**c and 11d** show stress ratio ($\eta = q/p\prime$;, where q is deviatoric stress, and $p\prime$ is the mean stress) versus dilatancy for the selected tests on the S1, S3, and S2 samples. Fig. 11**e** shows the volumetric strain versus axial strain for evaluating dilatancy. Of note, specimens from sample S2 were less dilatant than those from S1, and S3 at the same confining stress, which is consistent with the lower peak shear strength for S2 specimens. Fig. 11**c and 11d** also illustrate how the maximum dilatancy (D_{min}) was evaluated to investigate the dilation potential of these soils, given an initial state. The stress ratio at critical state (M_{tc}) is close to 1.55, which is consistent with the friction angles at residual conditions previously discussed. Fig. 11**f** shows the plot of D_{min} versus the initial state parameter (ψ_0) to calculate the dilatancy index χ according to $D_{min} = \chi\psi_0$, where χ can be thought of as a kinematic parameter related to the potential of the particulate materials to dilate or re-accommodate particles (Macedo and Vergaray, 2022; Jefferies and Been, 2015). The value of χ for natural uncemented sands is typically between 3 and 4. Interestingly, the χ values for the S1/S3 and S2 are 10.8, and 5.8, respectively. These values are significantly higher than those in natural sands, which may suggest some remaining cementation in the tested specimens after the flushing processes, i.e., F3PV and F9PV specimens. The higher χ value in the S1and S3 specimens also suggests higher remaining cementation as compared to the S2 specimens, which is consistent with the higher brittleness of the S1and S3 specimens. Later in the manuscript (section 4.2.2), we relate the observations on dilatancy just discussed with the cyclic response of the examined materials.

4.2. Dynamic loading behaviors

4.2.1. Dynamic material properties

Resonant column tests were performed on the intact samples of collapsible soil type B (i.e., S1 and S2 specimens) at their natural moisture content and on the RW specimens from sample S1. The specimens were placed in a resonant column device and tested for the low-amplitude shear modulus (G_{max}) and the low-amplitude material damping ratio as well as the variations of shear modulus (G) and the material damping with shear strain. The initial dimension for the tests were 5.0 cm in diameter and 10.5 cm in height. Table 4 shows additional relevant information regarding the test setup. Fig. 12 shows the resonant column results for the I-S1 specimen (Fig. 12a, b), the I-S2 specimen (Fig. 12c, d), and the RW-S1 specimen (Fig. 12e, f) at different confining stresses. The results show that at a given shear strain, G increases, and the damping ratio decreases with increasing confinement. The results in Fig. 12 were used to fit the G_{max} experimental data to the functional form in Equation (1):

$$G_{max} = A_g \left(\frac{\sigma\prime}{P_a}\right)^{n_G} \quad (1)$$

where A_g and n_G are fitting parameters that depend on the material, $\sigma\prime$ is the isotropic confining effective stress, and P_a is the atmospheric pressure. A_g is indicative of the stiffness of a material for a given $\sigma\prime$, and it is dependent on the material properties (e.g., gradation, angularity, density, and cementation). The parameter n_G is a measure of the increase in G_{max} with mean effective stress.

The calculated A_g for the I-S1, I-S2, and RW-S1 specimens are 535 MPa, 430 MPa, and 96 MPa, respectively. Fig. 13**a** – which also shows for reference the G_{max} inferred from geophysical tests in Fig. 6**b**. The A_g reduction from 535 to 96 MPa between intact S1 sample and RW sample (at a similar density) is a measure of the impact of cementation on G_{max}. The n_G of the RW specimen is 0.47, which is consistent with the typical value for sands (ranging from 0.45 to 0.55). However, the intact specimens showed lower n_G values (0.28 for I-S1 and 0.32 for I-S2), which indicates that the change in G_{max} due to the changes in σ are comparatively less pronounced for cemented sands. The cementation is a major contributor to stiffness and is not nearly as affected with an increase in confining pressure. Therefore, a low n_G and high Ag value for the intact specimens (compared to the RW specimen and typical values for sand) is a direct result of the high salt cementation in the intact specimens. More specifically, the Ag and n_G values indicate higher cementation in the specimen from sample S1 compared to the specimen from sample S2, which is consistent with the previous observations on the stress–strain curves on triaxial tests. Fig. 13**b** show the variation of damping ratio versus confinement for the three specimens. The minimum damping ratio is not largely affected by cementation, which is in contrast with the observations for G_{max}. In addition, the minimum damping ratio decreases with the increase of the confining pressure, which is consistent with observations in natural sands.

Fig. 14**a** shows the variation of G versus shear strain for tests conducted on I-S1, I-S2, and RW-S1specimens under an effective stress of 414 kPa, highlighting the significant different G values in the RW specimen compared to the I specimens. Fig. 14**b** shows the normalized shear modulus

Table 4
Properties of intact and reconstituted specimens for Resonant Column Tests for Collapsible Soil Type B.

Specimen ID		Vertical Stress (kPa)	Dry density (g/cm^3)	Void Ratio (e)
I	S1/ S3	400	1.63	0.62
RW		200	1.62	0.64
		400	1.58	0.67
		800	1.61	0.64
RC		200	1.59	0.67
		400	1.57	0.69
		800	1.63	0.63
I	S2	400	1.59	0.67

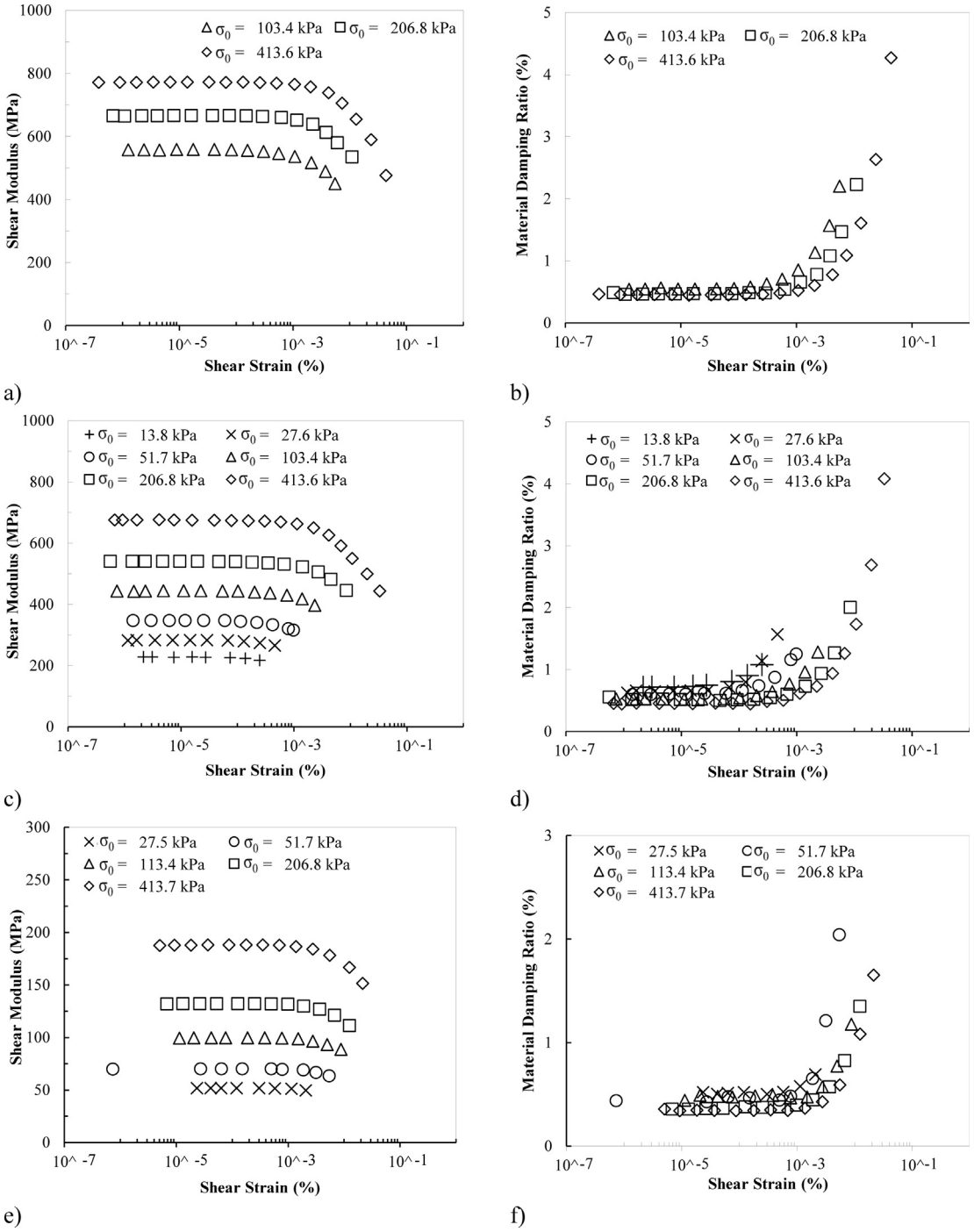

Fig. 12. Shear modulus and damping vs shear strain curves for different levels of mean effective stresses for the S1 intact specimen (a and b), S2 intact specimen (c and d) and S1 reconstituted RW specimen (e and f).

(by G_{max}) and damping ratio curves versus shear strain considering the tests on I and RW specimens. The normalized shear modulus (G/G_{max}) curves show a similar trend between the intact specimens (I-S1 and I-S2) and the "RW" specimen. Interestingly, the (G/G_{max}) and damping curves for the "I" and "RW" specimens are consistent with the natural sands bounds in Seed and Idriss (1970), which are included in Fig. 14**b** for comparison. Thus, even though G shows different significant values (Fig. 14**a**), the normalized G/G_{max} curves have a common non-linear response to increasing shear strains, suggesting that normalized (G/G_{max}) curves for natural sands can be used in seismic site response assessments of deposits with collapsible soils.

4.2.2. Cyclic direct simple shear test and liquefaction resistance

Cyclic direct simple shear (CDSS) tests were also performed to investigate the cyclic response and liquefaction

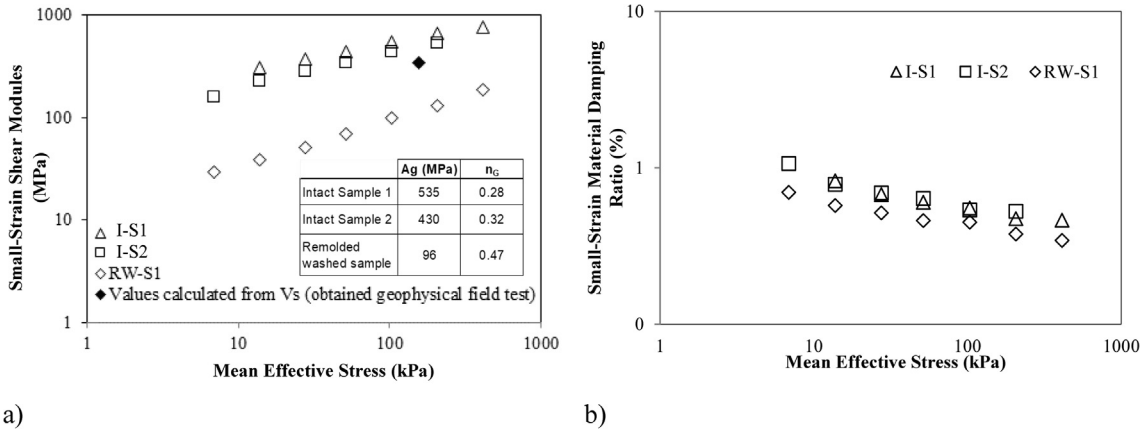

Fig. 13. Resonant column results for intact (I) and remolded washed (RW) samples. a) Small- strain shear modulus vs mean effective stress, b) Small-strain material damping ratio vs mean effective confinemen.

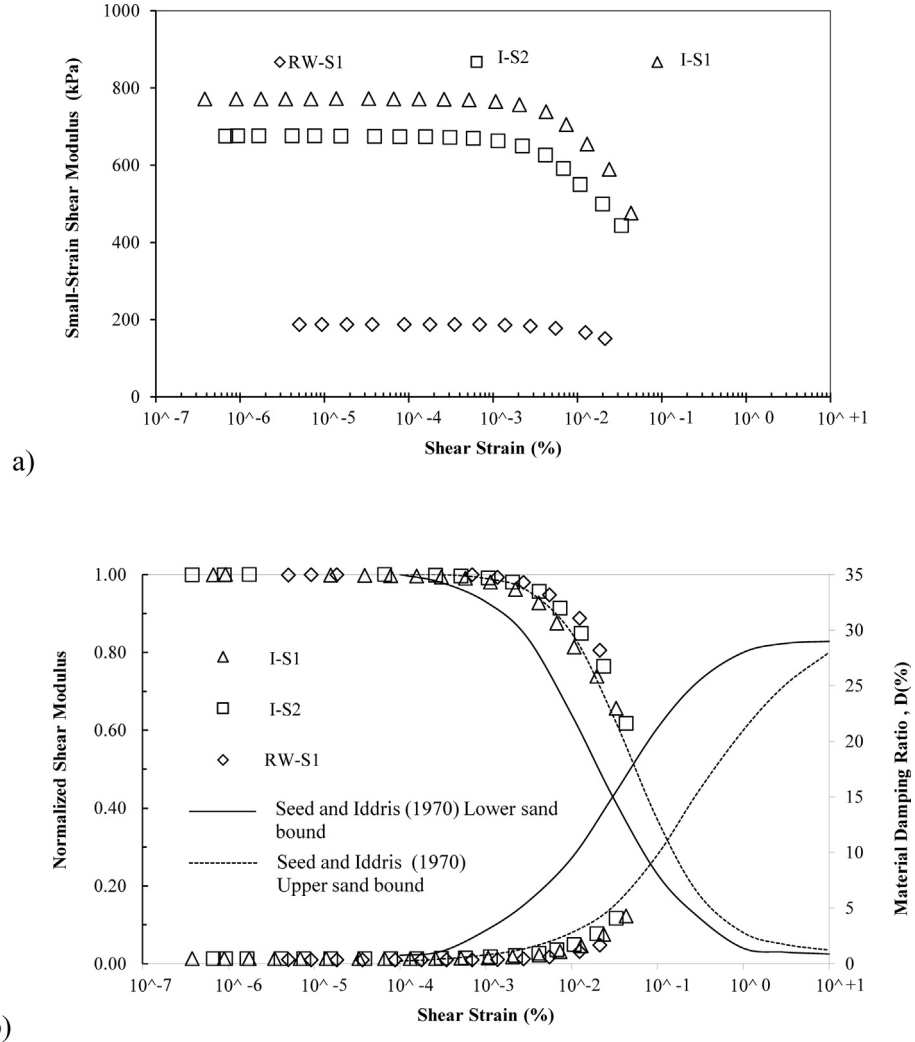

Fig. 14. Shear modulus and damping. a) Small-strain shear modulus vs strain, b) normalized shear modulus and damping curves for the tested materials along with the curves from Seed (1970).

Table 5
Properties of reconstituted washed specimens for Cyclic Simple Shear Tests for Collapsible Soil Type B.

Specimen ID		Vertical Stress (kPa)	Initial static bias (α)	Cyclic Stress Ratio (CSR)	Dry density (g/cm^3)	Void Ratio (e)
RW	S1/ S3	100	0.00	0.45	1.60	0.65
			0.00	0.50	1.60	0.66
			0.00	0.55	1.60	0.66
			0.00	0.65	1.60	0.66
			0.00	0.75	1.59	0.66
			0.00	0.90	1.60	0.66
		200	0.10	0.35	1.60	0.66
			0.10	0.40	1.60	0.65
			0.00	0.35	1.60	0.66
			0.10	0.30	1.60	0.66
			0.10	0.50	1.59	0.66
		400	0.00	0.35	1.61	0.65
			0.00	0.30	1.60	0.66
			0.00	0.20	1.60	0.66
			0.10	0.30	1.60	0.66
			0.10	0.35	1.60	0.66
			0.10	0.25	1.60	0.66
			0.10	0.40	1.60	0.65

resistance curves of the materials considered in this study. To simulate a post-collapse state due to the dissolution of salt when saturated prior to cyclic loading, the CSS tests were performed on collapsible soils type B, using RW-S1 specimens at the same dry density as the intact sample as shown in Table 5**,** and initial dimensions were 10.14 cm diameter and 2.5 cm height at the beginning of the tests**.** The procedure consisted of consolidating the specimens to a desired vertical stress, with or without an initial static shear stress. The magnitude of the initial static shear stress is defined by alpha, the ratio of the initial static shear stress to the initial vertical effective stress. Once the consolidation was complete; the vertical plate loading was locked in place (constant height testing), and the bottom plate was sheared under a harmonic sinusoidal loading at a frequency of 0.1 Hz, with amplitude characterized by a defined cyclic stress ratio (CSR is the ratio of the cyclic shear stress to the initial vertical effective stress).

Fig. 15 shows the typical responses observed during the CDSS tests, including the shear stress evolution (Fig. 15**a**), the accumulated shear strain (Fig. 15**b**), the vertical shear stress evolution (Fig. 15**c**), and the shear stress/strain loops (Fig. 15**d**). Fig. 15**e** shows the change in the normalized vertical stress, which is a proxy for the excess pore pressure generation, and Fig. 15**f** shows the normalized vertical stress versus shear strain. The tests, in general, showed a large cyclic resistance to liquefaction. Most specimens did not reach a normalized excess pore pressure ratio of unity (e.g., Fig. 15**e**). Therefore, a deformation criterion based on 5 % double amplitude axial strain criteria was chosen to identify the occurrence of liquefaction.

Fig. 16 shows the number of cycles to the "liquefaction" criterion plotted against the applied CSR for all the CSS tests performed in this study. We observed a decrease in the cyclic resistance of the tested materials with increasing confining stress, which is consistent with the behavior of typical sands. Applying an initial shear stress during the consolidation phase resulted in a minor increase in the number of cycles to reach liquefaction, which is observed in Fig. 15 for the confinement of 400 kPa. This is again consistent with previous studies on natural sands (e.g., Idriss and Boulanger, 2008).

The cyclic resistance for the collapsible soils tested in this study is larger compared to the cyclic resistance of natural sands; this is illustrated in Fig. 16, in which the cyclic resistance values from Toyoura and Monterrey sands. Although these natural sands were tested at high relative densities, such as the Toyoura sand with $D_r = 90\%$ at $\sigma'_3 = 100$ kPa (Yamamoto et al., 2009) and the Monterey sand with $D_r = 80\%$ at $\sigma'_3 = 80$ kPa (Wu et al., 2004), their cyclic resistances are generally lower as compared to values obtained from our tests. More specifically, the cyclic resistance values for the natural sands are lower than the cyclic resistance of the collapsible soil tested at 100 kPa and comparable to the cyclic resistance of the collapsible soils tested at 200 kPa and 400 kPa. These results are consistent with the large state-dilatancy parameter (χ) that was previously estimated for S1 specimens, which may cause higher strengths due to the large scaling of dilatancy given an initial state, influenced by the initial cementation.

5. Conclusion

This study discussed the collapse behavior and the static and cyclic response of collapsible salty sands sampled from an area with high seismicity on the Peruvian coast. The geotechnical characterization of the collapsible soils was performed through a series of laboratory and in-situ testing. The laboratory tests program consisted of oedometer consolidation, direct shear, consolidated undrained and consolidated drained triaxial, resonant column, and cyclic direct simple shear tests on intact and reconstituted speci-

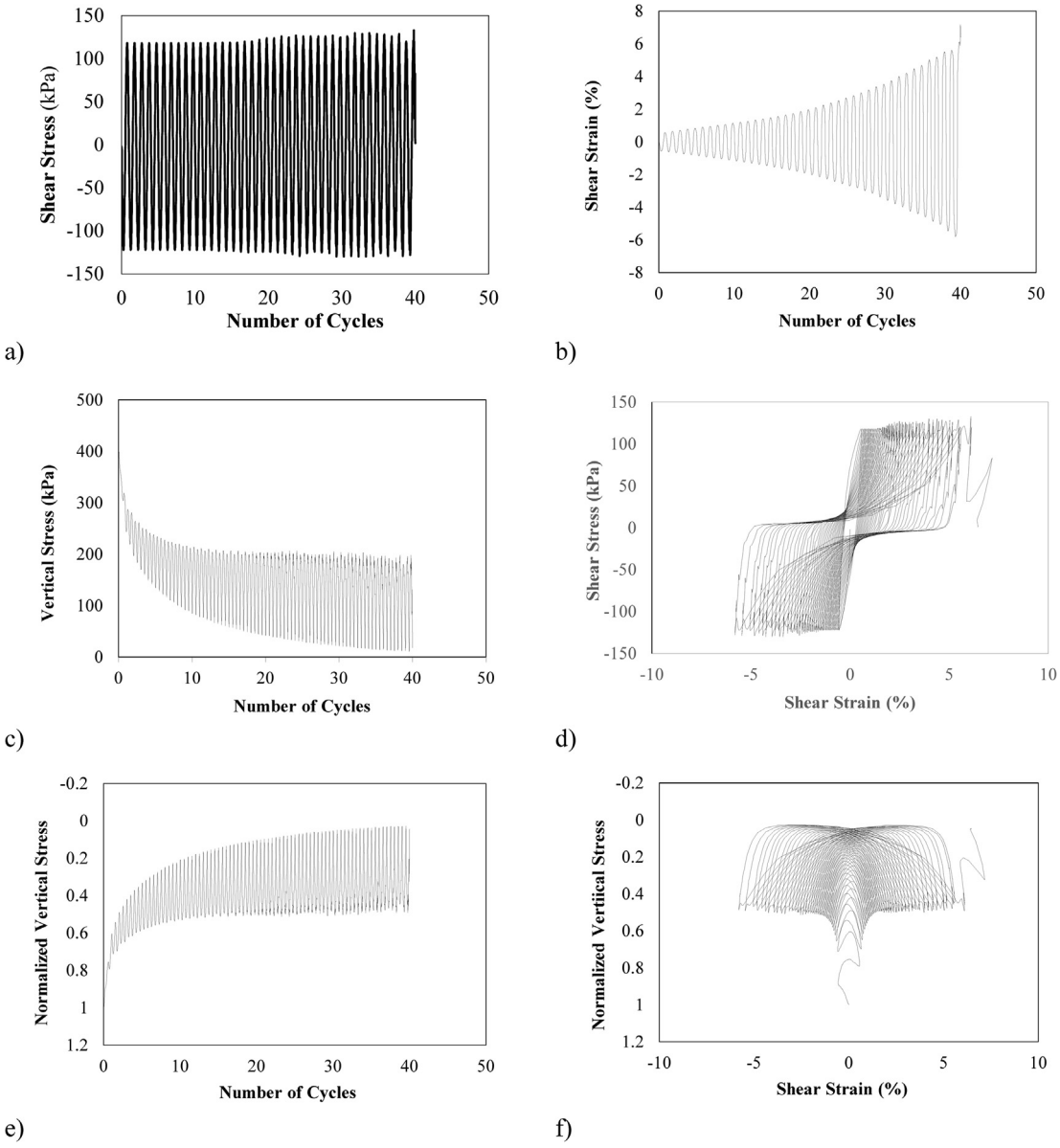

Fig. 15. Results of a CSS test for CSR = 0.30 at 400 kPa and alpha = 0.0 for S1 reconstituted washed (RW) samples of Collapsible Soils Type B. a) shear stress vs number of cycles, b) vertical stress vs number of cycles, c) normalized vertical stress vs number of cycles, d) shear strain vs number of cycles, e) shear stress vs shear strain, and f) normalized vertical stress vs shear strain.

mens. The in-situ testing/observations consisted of boreholes, test pits, Standard Penetration Tests, shear wave velocity measurements using Multichannel Analyses of Surface Waves, downhole permeability tests (i.e., Lefranc tests), and plate loading tests. Given the scarce information on the geotechnical characterization of salty sand collapsible soils in seismic areas, this study strives to serve as a useful reference for future studies on the static and cyclic behavior of such soils.

The direct shear tests showed a contractive behavior for collapsible soil Type A and a dilative behavior for collapsible soil Type B. These findings are consistent with the higher collapse potential and the looser state of collapsible soil Type A as determined from the oedometer tests, standard penetration tests, and plate loading tests. The combined results from the aforementioned tests indicate that in a dry state, these soils have a relatively high peak strength and initial stiffness, but in the presence of water, the precipitate bonds between grains can dissolve, causing the loose, high void ratio structure to collapse leading to high deformations.

The triaxial tests on intact and reconstituted specimens from collapsible soil Type B revealed a decrease in the brittleness index as the cementation is removed either by flushing intact specimens with water or washing sands prior to reconstituting specimens. Despite the reduction in the dif-

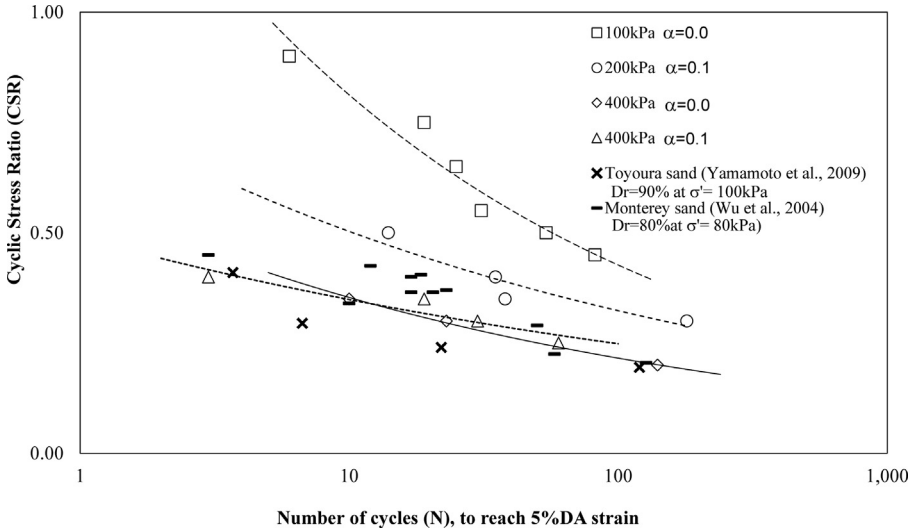

Fig. 16. Liquefaction resistance curve for Collapsible Soils Type B at different confining stresses compared with results for natural sands.

ference between the peak and residual strength with decreased degrees of cementation, the flushing/reconstitution processes had a minimal impact on the residual strength. The similar residual strength for a given confinement level is consistent with the critical state soil mechanics framework. This suggests that all the samples were in a "post-collapse" modified structure due to either post-shearing collapse in the intact specimens or reconstitution for the crushed and washed specimens.

The dilation potential was evaluated using the critical state soil mechanics framework; the results showed that the dilation potential index for S1and S3 specimens ($\chi = 10.8$) is higher than that for S2 specimens ($\chi = 5.8$) and typical values for clean sands ($\chi = 3$ to 4). These results are consistent with the larger brittleness index values for S1 and S3 specimens compared to S2 specimens and can be attributed to the higher cementation in S1 and S3 specimens compared to S2.

The resonant column tests revealed that the cementation is a major contributor to stiffness, with A_g measured in the intact specimens approximately-six times larger than that of the washed specimens. Furthermore, the low n_G value combined with a large A_g for specimen S1 compared to S2 is indicative of more cementation in S1, which is consistent with observations from the other tests. The G/G_{max} and damping ratio curves for the collapsible soils are consistent with curves upper and lower bounds for natural sands, respectively. This suggests that the previously reported G/G_{max} for natural sands can be used for site response analyses of sites that involve collapsible soils.

The CDSS tests showed a decrease in the cyclic resistance (or liquefaction resistance) of the tested materials with increasing confining stress and a minor increase of the cyclic resistance when initial shear stress is applied, which is consistent with the behavior of natural sands. However, the cyclic resistance for the collapsible soils tested in this study is generally larger compared to the cyclic resistance of natural sands, even when the natural sands are tested at a high density. These results are consistent with the large dilation potential index estimated for the specimens tested in the CDSS device, which in turn are influenced by the initial cementation.

Acknowledgment

The authors would like to acknowledge the contributions of Prof. Kenneth Stokoe and Ph.D. student Zhongze "Steve" Xu at the University of Texas at Austin for performing the Resonant Column testing and assisting with the analysis of the results. Their efforts are greatly appreciated. The authors would also like to thank the support of the Knight Piésold, Lima office for collecting the soils analyzed in this study during the geotechnical site investigation campaign.

References

Alonso, E.E., Gens, A., Josa, A., 1990. A constitutive model for partially saturated soils. Géotechnique 40, 405–430.

Al-Rawas, A., 2000. State-of-the-Art Review of Collapsible Soils. Science and Technology, Special Review.

Assadi-Langroudi, A., 2014. Micromechanics of collapse in loess. University of Birmingham.

Bishop, A.W., 1971. Shear strength parameters for undisturbed and remolded soil specimens, in: Roscoe Memorial Symp., pp. 3–58.

Cerato, A.B., Miller, G.A., Hajjat, J.A., 2009. Influence of clod-size and structure on wetting-induced volume change of compacted soil. J. Geotech. Geoenvironmental Eng. 135, 1620–1628.

Cui, Y.J., Delage, P., 1996. Yeilding and plastic behaviour of an unsaturated compacted silt. Géotechnique 46, 291–311.

Cui, Y.-J., Terpereau, J.-M., Marcial, D., Delage, P., Antoine, P., Marchadier, G., Ye, W.-M., 2004. A geological and geotechnical characterisation of the loess of Northern France. Advances in Geotechnical Engineering: The Skempton Conference. Thomas Telford Publishing, London, UK, pp. 417–428.

Delage, P., Audiguier, M., Cui, Y.-J., Howat, M.D., 1996. Microstructure of a compacted silt. Can. Geotech. J. 33, 150–158.
Derbyshire, E., Mellors, T.W., 1988. Geological and geotechnical characteristics of some loess and loessic soils from China and Britain: A comparison. Eng. Geol. 25, 135–175. https://doi.org/10.1016/0013-7952(88)90024-5.
El Howayek, A., Huang, P.-T., Bisnett, R., Santagata, M.C., 2011. Identification and behavior of collapsible soils. Joint Transportation. Res. Program.
Fan, X., Xu, Q., Scaringi, G., Li, S., Peng, D., 2017. A chemo-mechanical insight into the failure mechanism of frequently occurred landslides in the Loess Plateau, Gansu Province. China. Eng. Geol. 228, 337–345. https://doi.org/10.1016/j.enggeo.2017.09.003.
Fear, C.E., Robertson, P.K., 1995. Estimating the undrained strength of sand: a theoretical framework. Can. Geotech. J. 32, 859–870.
Feda, J., 1966. Structural stability of subsident loess soil from Praha-Dejvice. Eng. Geol. 1, 201–219.
Feda, J., 1988. Collapse of loess upon wetting. Eng. Geol. 25, 263–269.
Fredlund, D.G., Gan, J.K.M., 1995. The collapse mechanism of a soil subjected to one-dimensional loading and wetting, in: Genesis and Properties of Collapsible Soils. Springer, pp. 173–205.
Haeri, S.M., Garakani, A.A., Khosravi, A., Meehan, C.L., 2014. Assessing the hydro-mechanical behavior of collapsible soils using a modified triaxial test device. Geotech. Test. J. 37, 190–204.
Hailemariam, H., Al-Janabi, A., Wuttke, F., Wagner, N., 2015. Wave based monitoring of water-driven deterioration process of unsaturated, stressed collapsible soils, in: Proceedings of the International Symposium Non-Destructive Testing in Civil Engineering (NDT-CE). Berlin, Germany: BAM, TU Berlin. pp. 1–4.
Houston, S.L., Houston, W.N., Zapata, C.E., Lawrence, C., 2001. Geotechnical engineering practice for collapsible soils, in: Unsaturated Soil Concepts and Their Application in Geotechnical Practice. Springer, pp. 333–355.
Houston, S.L., Mahmoud, H.H.H., Houston, W.N., 1995. Down-hole collapse test system. J. Geotech. Eng. 121, 341–349. https://doi.org/10.1061/(ASCE)0733-9410(1995)121:4(341).
Idriss, I.M., Boulanger, R.W., 2008. Soil liquefaction during earthquakes. Earthquake Engineering Research Institute..
Jefferies, M., Been, K., 2015. Soil liquefaction: a critical state approach, 2nd ed. CRC Press.
Kalantari, B., 2013. Foundations on collapsible soils: a review. Proc. Inst. Civ. Eng. Eng. 166, 57–63.
Karam, J.-P., Cui, Y.-J., Tang, A.M., Terpereau, J.-M., Marchadier, G., 2009. Experimental study on the cyclic resistance of a natural loess from Northern France. Soils Found. 49, 421–429.
Li, Y., He, S., Deng, X., Xu, Y., 2018. Characterization of macropore structure of Malan loess in NW China based on 3D pipe models constructed by using computed tomography technology. J. Asian Earth Sci. 154, 271–279. https://doi.org/10.1016/j.jseaes.2017.12.028.
Li, P., Vanapalli, S., Li, T., 2016. Review of collapse triggering mechanism of collapsible soils due to wetting. J. Rock Mech. Geotech. Eng. 8, 256–274. https://doi.org/10.1016/j.jrmge.2015.12.002.
Liu, Z., Liu, F., Ma, F., Wang, M., Bai, X., Zheng, Y., Yin, H., Zhang, G., 2015. Collapsibility, composition, and microstructure of loess in China. Can. Geotech. J. 53, 673–686. https://doi.org/10.1139/cgj-2015-0285.
Mackechnie, W.R., 1989. Collapsible and swelling soils - Part 1: Collapsible soils. 12th International Conference on Soil Mechanics and Foundational Engineering. Rio De Janeiro, pp. 2485–2490.
Milodowski, A.E., Northmore, K.J., Kemp, S.J., Entwisle, D.C., Gunn, D.A., Jackson, P.D., Boardman, D.I., Zoumpakis, A., Rogers, C.D.F., Dixon, N., Jefferson, I., Smalley, I.J., Clarke, M., 2015. The mineralogy and fabric of 'Brickearths' in Kent, UK and their relationship to engineering behaviour. Bull. Eng. Geol. Environ. 74, 1187–1211. https://doi.org/10.1007/s10064-014-0694-5.
Noutash, M.K., Hajialilue, B.M., Cheshmdoost, M., 2010. Prepounding of canals as a remediation method for collapsible soils, in: Proceedings of the 4th International Conference on Geotechnical Engineering and Soil Mechanics, Tehran, Iran.
Qi, X., Xu, Q., Liu, F., 2018. Analysis of retrogressive loess flowslides in Heifangtai. China. Eng. Geol. 236, 119–128. https://doi.org/10.1016/j.enggeo.2017.08.028.
Rampino, C., Mancuso, C., Vinale, F., 2000. Experimental behaviour and modelling of an unsaturated compacted soil. Can. Geotech. J. 37, 748–763.
Reznik, Y.M., 1993. Plate-load tests of collapsible soils. J. Geotech. Eng. 119, 608–615.
Rinaldi, V.A., Redolfi, E.R., Santamarina, J.C., 1998. Characterization of collapsible soils with combined geophysical and penetration testing, in: Proceedings of the 1st International Conference on Site Characterization (ISC 98). Edited by PK Robertson and PW Mayne. AA Balkema Publishers, Atlanta, Ga. pp. 581–588.
Rogers, C.D.F., 1995. Types and distribution of collapsible soils, in: Genesis and Properties of Collapsible Soils. Springer, pp. 1–17.
Rollins, K.M., Jorgensen, S.J., Ross, T.E., 1998. Optimum moisture content for dynamic compaction of collapsible soils. J. Geotech. geoenvironmental Eng. 124, 699–708.
Sakr, M., Mashhour, M., Hanna, A., 2008. Egyptian collapsible soils and their improvement, in: GeoCongress 2008: Geosustainability and Geohazard Mitigation. pp. 654–661.
Seed, H.B., Idriss, I.M., 1970. Soil moduli and damping factors for dynamic response analysis. EERC.
Sivakumar, V., Wheeler, S.J., 2000. Influence of compaction procedure on the mechanical behaviour of an unsaturated compacted clay. Part 1: Wetting and isotropic compression. Géotechnique 50, 359–368.
Smalley, I.J., Mavlyanova, N.G., Rakhmatullaev, K.L., Shermatov, M.S., Machalett, B., O'Hara Dhand, K., Jefferson, I.F., 2006. The formation of loess deposits in the Tashkent region and parts of Central Asia; and problems with irrigation, hydrocollapse and soil erosion. Quat. Int. 152, 59–69. https://doi.org/10.1016/j.quaint.2006.02.018.
Song, B., Tsinaris, A., Anastasiadis, A., Pitilakis, K., Chen, W., 2017. Small-strain stiffness and damping of Lanzhou loess. Soil Dyn. Earthq. Eng. 95, 96–105. https://doi.org/10.1016/j.soildyn.2017.01.041.
Sotelo, G., Paihua, S., 2017. Estimate of Settlement of a Tailings Dam Founded on Collapsible Soils: Case Study, in: Proceeding of 4th International Seminar on Tailings Management. pp. 1–15.Vandanapu, R., Omer, J.R., Attom, M.F., 2016. Geotechnical case studies: emphasis on collapsible soil cases. Proc. Inst. Civ. Eng. Eng. 169, 103–110.
Sotelo, G., Orellana, S., Macedo, J., Jaffal, H., Espinoza, G., Xu, Z., El Mohtar, C., 2019. Geotechnical characterization of collapsible soils cemented by salts–a case study. Earthquake Geotechnical Engineering for Protection and Development of Environment and Constructions. CRC Press, pp. 5051–5060.
Wang, Q., Pufahl, D.E., Fredlund, D.G., 2002. A study of critical state on an unsaturated silty soil. Can. Geotech. J. 39, 213–218.
Wu, J., Kammerer, A.M., Riemer, M.F., Seed, R.B., Pestana, J.M., 2004. Laboratory study of liquefaction triggering criteria, in: 13th World Conference on Earthquake Engineering, Vancouver, BC, Canada, Paper.
Xu, L., Coop, M.R., 2016. Influence of structure on the behavior of a saturated clayey loess. Can. Geotech. J. 53, 1026–1037.
Xu, L., Coop, M.R., Zhang, M.S., Wang, G., 2018. The mechanics of a saturated silty loess and implications for landslides. Eng. Geol. 236, 29–42.
Yamamoto, Y., Hyodo, M., Orense, R.P., 2009. Liquefaction resistance of sandy soils under partially drained condition. J. Geotech. geoenvironmental Eng. 135, 1032–1043.
Zhou, A., Sheng, D., 2009. Yield stress, volume change, and shear strength behaviour of unsaturated soils: validation of the SFG model. Can. Geotech. J. 46, 1034–1045.

Further reading

Macedo, J., Vergaray, L., 2021. Properties of Mine Tailings for Static Liquefaction Assessment. Can. Geotech. J. 59 (5), 667–687. https://doi.org/10.1139/cgj-2020-0600.

INDECOPI, 2022. NTP 339.152 Norma Técnica Peruana. Método de Ensayo normalizado para la determinación del contenido de sales solubles en suelos y agua subterránea.

Yoshimi, Y., Tokimatsu, K., Kaneko, O., Makihara, Y., 1984. Undrained cyclic shear strength of a dense Niigata sand. Soils Found. 24 (4), 131–145.